Guillot-Ferriols, MT.; Rodriguez-Hernandez, J.; Correia, D.; Carabineiro, S.; Lanceros-Méndez, S.; Gómez Ribelles, JL.; Gallego Ferrer, G. (2020). Poly(vinylidene) fluoride membranes coated by heparin/collagen layer-by-layer, smart biomimetic approaches for mesenchymal stem cell culture. Materials Science and Engineering C: Materials for Biological Applications (Online). 117:1-12. https://doi.org/10.1016/j.msec.2020.111281

Poly(vinylidene) fluoride membranes coated by heparin/collagen layer-by-layer, smart biomimetic approaches for mesenchymal stem cell culture

Guillot-Ferriols M.[1,2], Rodríguez-Hernández J.C.[1], Correia D.M.[3,4], Carabineiro S.A.C.[5], Lanceros-Méndez S.[3,6,7], Gómez Ribelles J.L.[1,2], Gallego Ferrer G.[1,2]

[1] Centre for Biomaterials and Tissue Engineering (CBIT), Universitat Politècnica de València, 46022 Valencia, Spain

[2] Biomedical Research Networking Center on Bioengineering, Biomaterials and Nanomedicine (CIBER-BBN), Valencia, Spain

[3] Centre/Department of Physics, Universidade do Minho, 4710-057 Braga, Portugal

[4]Centre of Chemistry, Universidade do Trás-os-Montes e Alto Douro, Vila Real 5000-801, Portugal

[5]LAQV-REQUIMTE, Department of Chemistry, NOVA School of Science and Technology, Universidade NOVA de Lisboa, 2829-516 Caparica, Portugal

[6] BCMaterials, Basque Center for Materials, Applications and Nanostructures, UPV/EHU Science Park, 48940 Leioa, Spain

[7]IKERBASQUE, Basque Foundation for Science, 48013 Bilbao, Spain

Abstract

The use of piezoelectric materials in tissue engineering has grown considerably since inherent bone piezoelectricity was discovered. Combinations of piezoelectric polymers with magnetostrictive nanoparticles (MNP) can be used to magnetoelectrically stimulate cells by applying an external magnetic field which deforms the magnetostrictive nanoparticles in the polymer matrix, deforming the polymer itself, which varies the surface charge due to the piezoelectric effect. Poly(vinylidene) fluoride (PVDF) is the piezoelectric polymer with the largest piezoelectric coefficients, being a perfect candidate for osteogenic differentiation. As a first approach, in this paper, we propose PVDF membranes containing magnetostrictive nanoparticles and a biomimetic heparin/collagen layer-by-

layer (LbL) coating for mesenchymal stem cell culture. PVDF membranes 20 % (w/v) with and without cobalt ferrite oxide (PVDF-CFO) 10 % (w/w) were produced by non-solvent induced phase separation (NIPS). These membranes were found to be asymmetric, with a smooth surface, crystallinity ranging from 65 % to 61 %, and an electroactive β-phase content of 51.8 % and 55.6 % for PVDF and PVDF-CFO, respectively. Amine groups were grafted onto the membrane surface by an alkali treatment, providing positive charges for the assembly of heparin/collagen layers by the LbL technique. Five layers of each polyelectrolyte were deposited, ending with collagen. Ninhydrin test and X-ray photoelectron spectroscopy (XPS) revealed the presence of free amines on the surface, indicating a homogeneous LbL coating. Human mesenchymal stem cells (hMSC) were used to test cell response in a short-term culture (1, 3 and 7 days). Nucleus cell counting showed that LbL favored cell proliferation in PVDF-CFO over non-coated membranes.

Keywords: Poly(vinylidene) fluoride; non-solvent induced phase separation; layer-by-layer; collagen; mesenchymal stem cells; piezoelectricity.

1. Introduction

Bone is a dynamic tissue which is constantly remodelling itself and has the ability to self-regenerate. It is a complex organ that plays many roles in the human body, including structural support, hematopoietic and immunological function or calcium homeostasis [1]. As human life expectancy has increased in the last decades, this has favored the appearance of musculoskeletal diseases, including critical size defects due to trauma or cancer, or bone resorption and formation imbalances, leading to osteoporosis [2]. These bone loss related disorders have a great impact on the patients' quality of life and are costly for national health systems, since hundreds of millions of people are affected around the world [3].

Bone autografts, which are currently the gold standard treatment, involve great challenges, such as the lack of healthy tissue, invasive surgeries and the transplant failures after short periods of time [4]. Tissue engineering (TE) approaches have arisen over the years as valid candidates for bone healing and regeneration and bone TE has shown the need for specific polymers able to reproduce the physiological characteristics of the tissue itself. The importance of smart materials has recently increased in this field. When exposed to an external stimulus, these polymers are able to reverse one or more structural or functional properties [5]. Apart from their physical properties, these materials can be tailored to mimic specific characteristics of extracellular matrix (ECM) components or growth factors [6].

Smart materials can be a suitable approach to reproducing bone's inherent piezoelectricity. This phenomenon was hypothesized by Fukada and Yasuda in the 60's and was described as a change in the electric polarization under an applied mechanical stress, due to the collagen fibers that form its ECM [7]. Since then it has been proposed as one of the mechanisms involved in bone's capacity to adapt to mechanical stress and tissue regeneration [5,8].

Poly(vinylidene) fluoride (PVDF), a piezoelectric material, has gained growing interest in bone TE approaches. PVDF is a semi-crystalline polymer with one of the highest known piezoelectric coefficients. PVDF has five crystalline phases, the β-phase being the most electroactive due to its net permanent dipole generated by the all-trans conformation (TTT). The strong dipole moment is produced by the difference between the electronegativity of the fluorine atoms and hydrogen atoms in its structure [9].

Processing conditions and solvents are determinant in PVDF's crystallization in the β-phase. The α-phase, the most frequently obtained, always results in melt crystallization at any temperature [10]. Uniaxial stretching of α-phase PVDF films is the most common way of inducing the β-phase [11], although crystallization below 70 ºC by polar solvents such as dimethylformamide (DMF) or dimethylacetamide (DMA) also produces highly porous β-phase membranes [12,13].

Non-solvent induced phase separation (NIPS) has been described as a method of β-phase crystallization below 70 ºC [14,15]. This technique consists of precipitating the polymer cast on a surface by immersing it in a coagulation bath containing a non-solvent. The polymer solvent, non-solvent coagulation bath, bath temperature, additives and evaporation times can all influence the membrane morphology, which can range from highly homogeneous porous membranes to finger-like asymmetric structures with a flat surface [16]. NIPS membranes, mostly used in water remediation applications, have been poorly explored in the TE field [17,18], despite their easy processing. We consider them to be excellent candidates for mesenchymal stem cell culture.

Piezoelectric polymers can be combined with magnetostrictive phases to induce an electric charge through the magnetoelectric effect. When an external magnetic field is applied, the deformation of the magnetostrictive phase transfers this deformation to the polymer matrix resulting in a dielectric polarization variation due to the piezoelectric effect [19]. This approach has been used in PVDF scaffolds, microspheres and electrosprayed fibers for electromechanical stimulation of osteogenic precursors [20–22].

PVDF's piezoelectric properties are of great interest for bone regeneration, although mimicking the cell's environment requires other factors and molecules, which can be added to the equation by coating them onto the polymer surface, for which layer-by-layer (LbL) has been postulated as an easy, cost-effective and reliable technique. LbL allows the controlled deposition of multilayers that imitate the organization of native tissues using natural polyelectrolytes, such as polysaccharides and proteins. These biomolecules are suitable candidates due their lack of cytotoxicity and their obvious mimicking of cell ECM, which triggers migration, growth and cell organization [23–25].

Collagen Type I is the main protein in bone ECM. As mentioned above, its structure confers bone's inherent piezoelectricity. It is positively charged at pH below its isoelectric point (5.5) [26]. Heparin, a highly sulphated polysaccharide, is involved in cell migration, proliferation and differentiation due to its ability to bind members of the major growth factor and signaling protein families, including Wnt,

hedgehog, bone morphogenetic protein (BMP), fibroblast growth factor (FGF) and vascular endothelial growth factor (VEGF) families [27].

Combination of heparin/collagen as polyelectrolytes has been studied previously on different substrates and cell types, from simple approaches, improving adhesion properties of polydimethylsiloxane (PDMS) [26] to using heparin property as anticoagulant to coat titanium surfaces, providing thromboresistance and rapid re-endothelialization [28–30] or PLLA electrosprayed fiber coatings for releasing neurotrophic factors [31]. Regarding mesenchymal stem cells (MSCs), heparin/collagen LbL has proven to be a versatile approach for multiple scopes. It has been used to induce human MSCs osteogenic differentiation and mineralization [32], to increase vascularization *in vivo* promoting MSCs differentiation to endothelial cells [33] or to enhance human MSCs immunomodulatory properties in combination with interferon-gamma, reducing its antiproliferative effect [34].

As a first approach, the objective in this study was to develop and characterize novel PVDF membranes, using the NIPS technique, with magnetostrictive nanoparticles coated by collagen/heparin layer-by-layer. To the best of our knowledge, this is the first time that PVDF membranes have been produced containing cobalt ferrite oxides (CFO) by the NIPS method. Membranes with and without CFO nanoparticles were successfully aminolyzed to provide positive surface charges for layer-by-layer deposition. Heparin and collagen layer-by-layer assembly was confirmed by means of field emission scanning microscopy (FESEM), atomic force microscopy (AFM) and Fourier-transformed infrared spectroscopy (FTIR). Heparin/collagen multilayers were initially tested *in vitro* using hMSC. A short-term cell culture (1, 3 and 7 days) was performed to assess cell adhesion and proliferation by nucleus and cytoplasm staining to confirm PVDF-CFO membranes suitability for future bone TE approaches.

2. Materials and methods

2.1. Membrane preparation by *non-solvent induced phase separation (NIPS)*

PVDF membranes with and without cobalt ferrite oxide (CFO) were prepared by non-solvent induced precipitation (NIPS) using deionized water as non-solvent. A 20 % (w/v) PVDF (*Solef® 6010 PVDF Homopolymer, Solvay)* solution was prepared by dissolving the PVDF in dimethylformamide (DMF) (synthesis grade; Scharlab) at 60 °C under stirring. For the preparation of the composite solution (PVDF-CFO), cobalt ferrite oxide mangnetostrictive nanoparticles (CFO MNP) were used with diameters ranging from 35 to 55 nm (Nanoamor) at a concentration of 10 % (w/w). This concentration proved to be the most appropriate to induce a magnetoelectric response in PVDF [35]. CFO MNP were dispersed in DMF solvent and citric acid (Sigma-Aldrich) (0.2 mg/g PVDF) in an ultrasound bath to help its dispersion and prevent agglomeration [35]. After 4 h, PVDF was added and stirred with a Teflon mechanical stirrer, keeping the solution in the ultrasonic bath at 60 °C until complete dissolution of the polymer.

PVDF solution was spread on a glass plate using a 750 µm casting knife and placed in a water bath at 25 °C for 30 minutes. After complete coagulation, the membranes were detached from the glass and were transferred to a new water bath to remove possible traces of DMF. The membranes were washed under shacking for 24h and then frozen at -80 ºC and lyophilized for 24 h, assuring the elimination of possible remaining DMF traces.

2.2. Heparin and collagen type I Layer-by-Layer

Membranes were aminolyzed in two steps. In the first, the membranes were treated with a 3.75 M NaOH (Scharlab) solution for 1 hour at room temperature to eliminate some fluorine and hydrogen atoms, creating an unsaturation in the PVDF backbone. They were then introduced in a solution of 1,4-diaminobutane dihydrochloride (DAB; Sigma-Aldrich) 1M in sodium carbonate (Sigma-Aldrich), with a final pH of 12, for 24 h at 55 °C to graft amine groups onto the membrane's surface. Membranes were washed with deionized water. The amount of the amino groups present on the surface was determined by the ninhydrin test, following the protocol described in [36]. Treated membrane disks of

4 mm diameter were then immersed in 2 mL of ninhydrin solution and incubated at 80 °C for 20 minutes. The solution was then diluted with 3 mL of 2-propanol (Scharlab) 50% (v/v) in deionized water. Absorbance was read at 570 nm in a Victor3 microplate reader (Perkin Elmer). Non-treated membranes were used as blanks and amine concentration was determined by a glycine standard curve. All measurements were performed in triplicate.

Positively charged PVDF surfaces were washed with ultrapure water pH 5 to protonate amine groups. LbL was performed alternating one layer of heparin (Sigma-Aldrich) and one layer of collagen type I (Advanced Biomatrix). Solutions were prepared at a concentration of 1 mg/mL using ultrapure water pH 5, adjusting final pH to 5 [32]. A volume of 70 µL of each solution was deposited on 8 mm diameter PVDF samples for 10 minutes. After washing with pH 5 ultrapure water, the complementary layer was deposited until 5 layers of each solution coated the surface.

2.3. Membrane characterization

2.3.1. Field Emission Scanning Electron Microscopy (FESEM)

Membrane structure (both surfaces and cross-section) and deposition of the heparin/collagen layers were evaluated by field emission scanning electron microscopy (FESEM) (Ultra 55, Zeiss) with an accelerating voltage of 1kV. The membranes were coated with platinum following a standard sputtering protocol for 90 s (JFC 1100, JEOL, Japan).

Membrane spherulite diameter was assessed from FESEM images. 100 spherulites from each of three different membranes, produced in three different synthesis, were measured using ImageJ software (National Institutes of Health, Bethesda, Maryland, USA).

2.3.2. Fourier Transformed Infrared Spectroscopy (FTIR)

Fourier transformed infrared spectroscopy (FTIR) was carried out to determine the presence of PVDF's most electroactive form, the β-phase. Measurements were performed by an ALPHA FTIR spectrometer (Bruker) in ATR mode from 4000 to 400 cm^{-1} at a wavenumber resolution of 4 cm^{-1}. Representative absorption bands at 840 cm^{-1} and 760 cm^{-1}, which correspond to the β and α phase

respectively, were identified and their content was determined using the procedure proposed by Gregorio and Cestari, yielding Eq. (1) [37].

The β-phase fraction, $F(\beta)$ is:

$$F(\beta) = \frac{A_\beta}{\left(K_\beta / K_\alpha\right) A_\alpha + A_\beta} \quad (1)$$

The method assumes that FTIR absorption follows the Lambert-Beer law, K_α and K_β, are the characteristic absorption coefficients at the characteristic wavenumbers of the α and β-phases (760 and 840 cm^{-1}, respectively). These were determined in reference [37] from samples containing only α or β-phase, obtaining values of 6.1×10^4 and 7.7×10^4 cm^2/mol, respectively. A_α and A_β are the measured absorbances at 760 and 840 cm^{-1} respectively.

Presence of collagen and heparin after layer-by-layer coating was also assessed by FTIR.

2.3.3. Differential Scanning Calorimetry (DSC)

Thermal properties of the membranes were evaluated by differential scanning calorimetry (DSC) using a DSC Pyris 1 (PerkinElmer) in a dry nitrogen atmosphere. Samples between 2 and 6 mg encapsulated in aluminium pans were used in the experiments. Scans were performed from 0 °C to 200 °C at a heating range of 20 °C/min. Degree of sample crystallinity (X_c) was determined using Eq. (2) [38]:

$$\Delta X_c = \frac{\Delta H_m}{w_{PVDF}(x\Delta H_\alpha + y\Delta H_\beta)} \quad (2)$$

where ΔH_m is the melting enthalpy of PVDF membranes measured in DSC and ΔH_α and ΔH_β are the melting enthalpies of a 100% crystalline sample in the α and β phases, whose values are 93.07 J/g and 103.4 J/g, respectively. w_{PVDF} is the mass fraction of PVDF within the membranes (provided by their magnetic properties), and *x* and *y* are the percentage of α and β phases present in the sample, obtained by FTIR measurements.

2.3.4. Vibrational Sample Magnetometer (VSM)

Magnetic properties of the composite membranes (PVDF-CFO) were evaluated using a Microsense 2 Tesla vibrating sample magnetometer (VSM). Magnetization loops M(H) were evaluated up to 18.5 kOe. To determine the real percentage of CFO in the composite samples, the saturation magnetization value of the pure CFO nanoparticles was compared with those obtained using Eq. (3) [19]:

$$CFO\ wt\ \%\ membranes = \frac{Saturation\ magnetization\ membranes}{Saturation\ magnetization\ pure\ CFO} x100 \quad (3)$$

The value of saturation magnetization of pure CFO being 60 emu/g.

Three different zones of the same PVDF-CFO membrane were evaluated to ensure homogeneous CFO distribution within the membrane matrix.

2.3.5. X-ray photoelectron spectroscopy (XPS)

Two-step amynolization was assessed by X-ray photoelectron spectroscopy by means of a XPS Kratos Axis Ultra HSA apparatus, which uses a micro-focused monochromatic Al Kα X-ray source (1486.6 eV) covering an analysing area of 300 x 700 μm (90 W power). Survey spectra were collected at a pass energy of 160 eV, step size of 1 eV, and dwell time of 200 ms with the spectrometer operated in hybrid lens mode. High-resolution C1s regional spectra were collected using a pass energy of 40 eV, step size of 0.1 eV, and dwell time of 200 ms. High-resolution regional spectra of N1s and O1s were collected using the same parameters, except for the dwell time, which was 1500 ms. High-resolution spectra envelopes were processed using CasaXPS software.

2.3.6. Determination of Heparin concentration

Heparin deposition on PVDF and PVDF-CFO membrane's surface after layer-by-layer was confirmed measuring its concentration by Taylor's blue colorimetric method using Glycosaminoglycan Assay Blyscan (Biocolor). LbL was performed in membranes with a surface of 1 cm^2 applying 1, 3 or 5

layers of heparin. Samples were labelled as H and the corresponding number of layers of the biomolecule. Shortly, membranes were soaked in 1 mL of Blyscan dye reagent containing 1,9-dimethylmethylene blue and incubated for 30 minutes under shacking at room temperature. After incubation, samples were washed with distilled water and transferred to a new eppendorf. 0.5 mL of dissociation reagent were added to favor heparin dissociation from 1,9-dimethylmethylene. Absorbance was read at 652 nm (Victor3 microplate reader; Perkin Elmer) transferring 100 μl of each sample to a 96-well plate. Heparin concentration was determined using a heparin calibration curve (0-5 μg). All measurements were performed in triplicate.

2.3.7. Atomic Force Microscopy (AFM)

Collagen layer deposition on PVDF membranes was confirmed by means of atomic force microscopy (AFM). Non coated PVDF samples and samples containing 1 (C1) and 5 bilayers (C5) were analysed. Atomic force microscopy was performed on a Multimode 8 (Bruker) operating in tapping mode in air. RFESPA silicon probes from Bruker were used with a force constant of 3 N/m and resonance frequency of 75 kHz. The tapping frequency was slightly lower than the resonance (around 10%), in which the phase signal was set to zero. The linear speed of the tip was set at 2 μm/s and the drive amplitude was modified to obtain an oscillation-free length of 700 mV. The ratio between setpoint and drive amplitude was maximized to obtain images with the least surface deformation (i.e. soft tapping).

2.4. Cell response

Human bone marrow mesenchymal stem cells (hMSC) (Promocell, Germany) were used to evaluate cell response. A short-term culture (1, 3 and 7 days) was carried out to check cell proliferation on PVDF and PVDF-CFO membranes coated by collagen/heparin layer-by-layer.

hMSC were expanded in a basal medium containing Dulbecco's Modified Eagles Medium (DMEM) high glucose (4.5 g/L) (Gibco) supplemented with 10% (v/v) foetal bovine serum (FBS; Gibco), 4 mM L-glutamine (Lonza), 10 mM non-essential aminoacids (Gibco), 10 mM sodium pyruvate (Gibco), 70 U/mL penicillin, 70 μg/mL streptomycin (P/S; Life technologies) and 0.25 μg/mL fungizone (Life

technologies), at 37 ºC in a humidified atmosphere with 5 % CO_2. All experiments were performed at passage 4.

After aminolyzing the membranes, 8 mm diameter disks were obtained and sterilized by UV exposition for 1 hour. PVDF membranes were then immersed in ethanol 70 % (v/v) for 20 minutes and washed 5 times with ultrapure water, last wash with pH 5 ultrapure water to protonate amine groups. Layer-by-layer was performed in sterile conditions, nonetheless, as pH adjustment of collagen solution required non-sterile conditions PVDF and PVDF-CFO membranes already coated were sterilized again using the same protocol.

PVDF and PVDF-CFO membranes, non aminolyzed, and glass slides coated with fibronectin from human plasma (Sigma-Aldrich) were used as controls to compare the effect of layer-by-layer coating with a conventional protein adsorption. Since the scope of our work was to compare the established fibronectin coating protocol with more complex approaches involving other biomolecules, non-coated surfaces were not used. All controls were coated after sterilization by incubation in a 20 μg/mL fibronectin solution for 1 hour at room temperature.

12 h before cell seeding, cells were starved in basal media containing 1 % (v/v) FBS to synchronize cell cycle. To study cell proliferation cells were seeded at a density of 8 x 10^3 cells/cm^2 in basal medium without FBS (3 replicates per group) to promote cell adhesion either to fibronectin or collagen. A 100 μL drop containing the right number of cells was deposited on the surface of the samples. After 3 h the required volume of basal medium and FBS for a final concentration of 10 % (v/v) were added to each well. Silicon rings were used to keep the membranes fixed on the bottom of the well. These rings were also used in glass slides controls. After 1, 3 and 7 days cells were fixed in a 4 % (v/v) paraformaldehyde solution (Panreac) for 20 minutes.

Cell proliferation was assessed by nuclei counting using nucleus and cytoplasm staining. Before staining, PVDF and PVDF-CFO membranes were treated with a 0.2 % (w/v) Sudan Black B solution for 40 minutes to avoid PVDF autofluorescence, which hinders image acquisition and quantification [39]. Membranes were washed 3 times with Dulbecco's Phosphate Saline Buffer (DPBS; Sigma-Aldrich). Subsequently, samples were permeabilized and blocked in 1 % (w/v) bovine serum albumin

(BSA; Sigma-Aldrich) solution in DPBS/0.1 % (v/v) Tween-20 (Sigma-Aldrich) for 1h at room temperature and incubated with Actin Red 555 Ready Probes reagent (Fisher Scientific) following manufacturer's instructions, then washed 3 times with DPBS/0.1 % (v/v) Tween-20 and incubated for 20 minutes with Hoechst (1:400; Thermo Fisher) in mounting medium.

Images of four representative fields of every sample were taken with a fluorescence microscope (Nikon Eclipse 80i) and analyzed using ImageJ software (National Institutes of Health, Bethesda, Maryland, USA). Cell number was expressed as the number of cells per square centimeter.
ImageJ software was also used to quantify cell spreading after 24h of cell culture. Briefly, masks of images were obtained by previous segmentation and cell area was measured for the scaled images. Approximately 60 cells per condition, from different replicates, were measured.

2.5. Statistical analysis

Statistical analysis was assessed by Graphpad Prism 6 software (Graphpad Software, United States). For cell counting data analysis, homoscedasticity was checked by Snedecor's F-distribution. T-test was used to find significant differences between each studied group. For cell spreading analysis, after checking homoscedasticity, a non-parametric Kruskall-Wallis test was performed to detect significant differences. Significance was accepted as $p\text{-}value < 0.05$

3. Results and discussion

3.1. Membrane characterization

The non-solvent induced precipitation technique can obtain a wide variety of membrane morphologies according to the different parameters involved in polymer precipitation. PVDF and PVDF-CFO membranes were produced using distilled water at 25 ºC as non-solvent and immersing them immediately in the coagulation bath to reduce air exposure to the minimum.

The non-solvent selection plays a crucial role in the final membrane morphology. Water is known to be a strong non-solvent for PVDF and leads to asymmetric structures like those shown in Figure 1. Membranes produced using harsh baths, e.g. water, exhibited a smooth surface, non-porous at the micrometer level, followed by macrovoids or finger-like structures which continued with a porous structure composed of spherulites, as can be seen in Figure 1(c). Top surface of image 1(c) is that of the smooth surface shown in image 1(b), while image 1(a) is of the bottom surface in contact with the casting glass.

PVDF precipitation into a membrane is governed by two events: liquid-liquid demixing and crystallization due to the semi-crystalline nature of PVDF [16]. The importance of these phenomena lies in the order in which they take place. Water-induced precipitation leads to rapid liquid-liquid demixing before crystallization, giving rise to asymmetric membranes such as those obtained [40].

Coagulation bath temperature also contributes to the membrane structure [41]. Higher temperatures up to 65 ºC provide a favorable condition for liquid-liquid demixing and tend to form larger finger-like structures, while low temperatures such as those used here reduce their formation, giving place to small macrovoids and sponge-like membranes similar to those obtained from soft non-solvents.

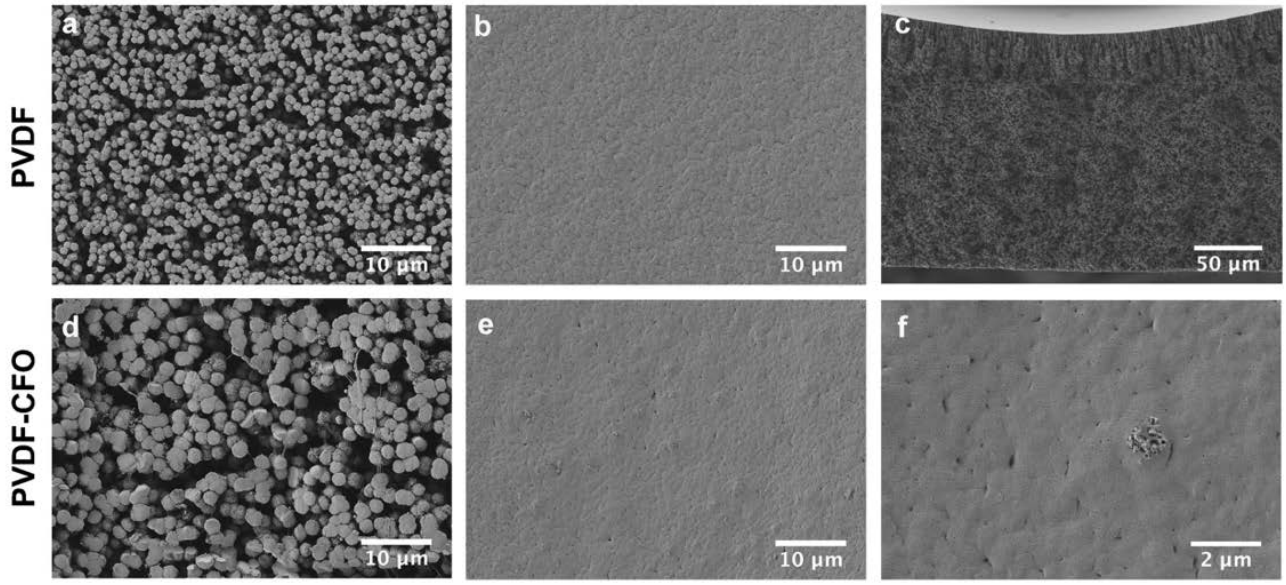

***Figure 1**. FESEM images of PVDF and PVDF-CFO NIPS membranes. **(a), (d)** Porous, bottom surface. **(b), (e)** Smooth, top surface of PVDF and PVDF-CFO membranes, respectively. **(c)** PVDF membrane cross-section showing the top finger-like structure and the underlying microporous structure formed by PVDF spherulites. **(f)** CFO trapped on PVDF-CFO top surface (magnification of image (e)).*

Adding CFO oxide did not modify the overall membrane structure, as shown in FESEM images 1(d) and (e). The difference in spherulite size can be seen in images 1(a) and (d). Measurements revealed that PVDF spherulite diameter was 0.99 ± 0.17 μm, while PVDF-CFO spherulites doubled theirs to 2.15 ± 0.42 μm. This difference could be explained by the addition of CFO nanoparticles to the initial solution. Supriya et al. [42] studied the effect of CFO MNP diameter on the performance of dielectric PVDF nanocomposites. They postulated that CFO nanoparticles are negatively charged, making them interact with the positively charged CH_2 bond, acting as a core and giving place to a core-shell structure formed by CFO and PVDF. They observed that the larger the CFO nanoparticle diameter, the larger the granular structures present in the PVDF nanocomposites and also that they were prone to agglomerate at larger diameters. It is plausible that CFO MNP aggregates could be acting as nucleation centers for the formation of PVDF spherulites, obtaining larger diameters than the PVDF membranes.

Lin et al [43] described the change of the spherulite diameter in PVDF membranes produced in 1-octanol baths, according to the precursor-solution preparation temperature. Lower temperatures favored a higher density of nuclei available for the initiation of crystallization. Although the solutions looked macroscopically similar, those at higher temperatures contained less undissolved and invisible pre-nucleation aggregates. Even if the applied temperature is the same, the presence of CFO in the solution requires different preparation methods, including mechanical stirring and ultrasounds for longer periods. This protocol may lead to fewer nuclei, reducing the crystallization points and increasing spherulite diameter.

Further experiments will be needed to confirm which of these hypotheses can explain the variation in spherulite diameter.

The main objective when producing PVDF cell culture supports able to subject cells to electrical stimulation during culture is to obtain electroactive phases. As mentioned in the Introduction, PVDF has 5 polymorphs, α, β and γ being the most important. α is a non-electroactive phase, due to antiparallel dipole packing within the unit cell (TGTG) [44]. All-trans (TTT) or T_3GT_3G structures present in β and γ phases, respectively, make them the most piezoelectric and give them very similar

conformations, which makes it difficult to distinguish between both phases using Fourier transformed infrared spectroscopy or X-ray diffraction peaks, due to their proximity. The β and γ phases usually show a typical peak at 840 cm^{-1}, which tends to form a shoulder at 833 cm^{-1} at a high γ phase contribution, while no such shoulder is shown for pure β phase [9]. Many authors agree in using 1234 cm^{-1} and 1279 cm^{-1} to differentiate between γ and β, respectively, since they are exclusive to each polymorph [44].

Synthesized membranes showed different FTIR spectra in the smooth and porous sides, as can be noted in Figure 2(a) and (b). The smooth surface was a mixture of α and β, in which characteristic non-polar phase peaks can be appreciated, 532, 614, 795, 975 cm^{-1} among others. 760 cm^{-1} is the most characteristic and was used to calculate the percentage of α polymorph present in the sample. A strong band at 840 cm^{-1} was present with no signs of 1234 cm^{-1} γ characteristic band, being only visible 1279 cm^{-1} in this region of the spectrum, corresponding to β-phase.

Eq. (1) was used to calculate the percentage of each phase, since this side will be used as a cell culture support for human mesenchymal stem cells. The percentages of β-phase were 51.8 % for PVDF and 55.6 % for PVDF-CFO membranes. It has previously been shown that including fillers in the PVDF matrix enhances β-phase crystallization and increases its percentage in the nanocomposites, compared to the PVDF structures [38]. Regarding the porous surface, the FTIR spectra showed a mixture of γ and β-phase, with no α-phase content. Characteristic peaks at 431, 776 and 1234 cm^{-1} revealed the presence of γ and peaks at 445, 840 and 1279 cm^{-1} reinforced β-phase. The strong band at 840 cm^{-1} with no shoulder at 833 cm^{-1} led to the conclusion that β is the main phase in the porous surface. Nonetheless, the γ-phase could be noted, giving rise to a mostly electroactive membrane, since the porous structure's contribution to the membrane was much greater than that of the smooth surface. As previously mentioned, the difficulty in distinguishing between both phases makes it difficult to quantify β-phase percentage by FTIR spectra only.

These findings agree with those obtained by Boccaccio et al. [45], who made an exhaustive analysis of PVDF membranes using DMF as solvent by the NIPS manufacturing method, assessing the PVDF phases by different FTIR techniques. They found that membranes were mostly β-phase in the finger-like structure, with a contribution of γ-phase to the porous part. The smooth surface, some microns thick, was composed of α and β, though no percentage of each phase was given. Other studies confirmed the presence of a mixture α and β phase on the membrane surface, although different solvents and coagulation bath temperatures were used [46,47].

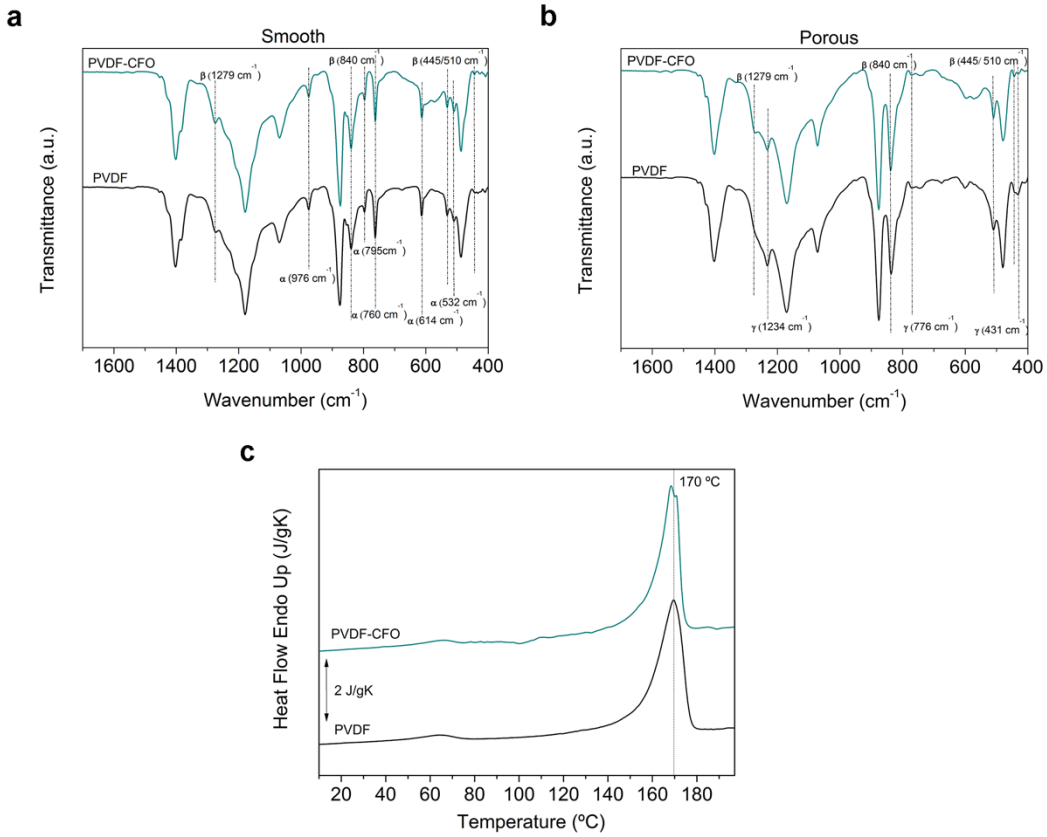

***Figure 2**. **(a)** Infrared spectra of smooth surface of PVDF and PVDF-CFO membranes where characteristic peaks of α and β phases are highlighted. **(b)** Infrared spectra of porous surface of PVDF and PVDF-CFO membranes where characteristic peaks of β and γ phases are highlighted. **(c)** DSC heating thermograms of PVDF and PVDF-CFO membranes.*

Differential scanning calorimetry was used to determine the crystalline fraction present in the studied sample. Differences in the melting temperatures (T_m) of PVDF crystalline phases can be used as an indicator of their presence in the sample, although they should be used as a complementary method to FTIR only, since T_m is also affected by crystalline defects and are especially present when the sample contains a filler [9].

Figure 2(c) shows the presence of the endothermic peaks around 170 ºC. PVDF membranes had their T_m at 170.2 ºC, while PVDF-CFO presented two endothermic peaks, the T_m being 168.4 ºC. The presence of more than one endothermic peak can be attributed to two phenomena: either the coexistence of two different crystalline phases in the same sample, or crystallite perfection. The presence of two endothermic peaks can only be seen in composite PVDF-CFO membranes. Since the coexistence of more than one polymorph has been described in both types of membranes by means of FTIR, the double endotherm peak present in PVDF-CFO must be due to different crystal sizes because of the presence of CFO.

Crystallinity (X_c) can be calculated applying Eq. (2) using the melting enthalpies extracted from the DSC analysis. No contribution from the α-phase was assumed, since this phase, measuring only a few micrometres, is only present in the smooth surface. The results show that PVDF membranes had higher crystallinity (66 %) than PVDF-CFO membranes (61 %). These high contents indicate that crystallization also occurs during polymer precipitation, even though liquid-liquid demixing takes place first. Low temperature coagulation baths favour a lower mass exchange between solvent and non-solvent, delaying liquid-liquid demixing and giving more time to the crystallization process [47].

The difference in X_c between PVDF structures with and without CFO MNP was explained by Martins et al. [38]. PVDF composites tended to have a lower degree of crystallinity than pristine PVDF. As shown by the two endothermic peaks in the DSC, composite membranes possessed more crystal defects, which can contribute to lower X_c.

Incorporating CFO nanoparticles into the membranes was assessed by the Vibrational Sample Magnetometer (VSM), measuring the magnetic response. VSM can be used to determine the real

content of CFO nanoparticles present in a sample and therefore nanoparticle loss during the composite manufacturing process [19,22].

Figure 3(a) shows the typical hysteresis loop for PVDF-CFO nanocomposites. Magnetization increased when the intensity of the applied field was raised until it saturated. The CFO content was calculated by Eq. (3), being 9.04 % ± 0.01 % in the sample, starting from a 10% (w/w) concentration in the polymer solution. These data were obtained by measuring the magnetic response in three different zones of the same membrane, ensuring the correct distribution of the MNP within the composite sample. The cross-section of PVDF-CFO membrane in Figure 3(b) and (c) shows good CFO MNP distribution within the polymer matrix, as confirmed by VSM. Nevertheless, cobalt ferrite oxide tends to form aggregates up to 1 μm, as can be seen in the FESEM image in Figure 3(c).

In addition to being a simple process, these data show that NIPS is a valid technique for incorporating CFO into the polymer matrix. Unlike other techniques for producing PVDF nanocomposites, e.g. electrospinning [22], electrospray [19] or solvent casting [20], in which nanoparticle loss is more than 30 %, NIPS can incorporate up to 90 % of the MNP.

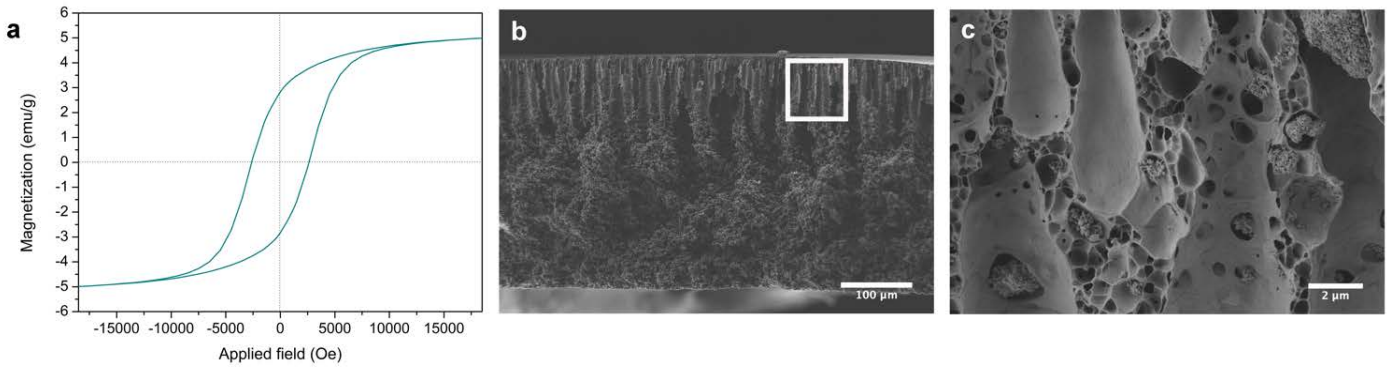

Figure 3. (a) *Room-temperature hysteresis loop of PVDF-CFO membranes.* ***(b)*** *Cross-section FESEM image of a PVDF-CFO membrane.* ***(c)*** *Magnification of the square zone in (b) where aggregation of CFO nanoparticles can be seen within the polymer matrix.*

3.2. Amine graft characterization

PVDF is a widely used fluoropolymer due to its strong chemical resistance, which means it is difficult to modify its chemical structure, claiming the need of aggressive treatments. A two-step treatment

was used to graft free amine groups onto the PVDF surface. PVDF and PVDF-CFO membranes were first immersed in a 3.75 M NaOH solution for 1 hour at room temperature to dehydrofluorinize the polymer, followed by the formation of a conjugate double bond or polyene structure (C=C). After NaOH treatment the membranes became brownish, a macroscopic indicator of PVDF fluorine and hydrogen elimination [48].

This bond can be attacked by specific molecules, such as 1,4-diaminobutane, which contains two primary amine groups. One group is able to bond to the polyene structure while the other will remain free to act in an acidic pH medium as a positive charge on the surface to promote the union of the first heparin layer. Incubation with 1,4-diaminobutane was performed for 24 h at 55 ºC, following Algieri et al. [49] optimized protocol.

An XPS analysis was carried out to study the efficiency of the chemical modification on both the PVDF and PVDF-CFO surfaces. The scan spectra of C1s, F1s, O1s and N1s are shown in Figure 4. The elemental composition of all samples is given in Table 1.

The C1s spectra of PVDF and PVDF-CFO before and after NaOH chemical treatment are shown in Figure 4(a). Whatever the surface, both untreated PVDF and PVDF-CFO display the main C1s PVDF characteristic peaks at 286.4 eV and 291.4 eV attributed to the CH_2 and CF_2 groups, respectively, and the peak at 285.0 eV assigned to the C-C group [50,51]. Some differences were found in the intensity of the XPS scans in the NaOH treated samples. The intensity of the characteristic CF_2 and CH_2 peaks was seen to fall, while the C-C group's characteristic peak rose, indicating the loss of hydrogen and fluorine atoms after the post-chemical treatment with NaOH. No significant changes were seen after the DAB chemical treatment, showing the main C1s peaks PVDF characteristics. The C-C group was attenuated in PVDF-CFO composites on both treated and untreated surfaces (Figure 4(a) and 4(b)).

Two peaks at 688 eV and 684 eV associated to the C-F groups [51,52] can be seen in the F1s scan spectra in Figure 4c. The peak at 533 eV at O1s is attributed to oxygen groups from the water formed during the dehydrofluorination process (Figure 4e), as reported in [49]. The DAB reaction with the polymer chain is proven by the assigned peak at 400 eV (Figure 4f), attributed to NH_2 groups [53].

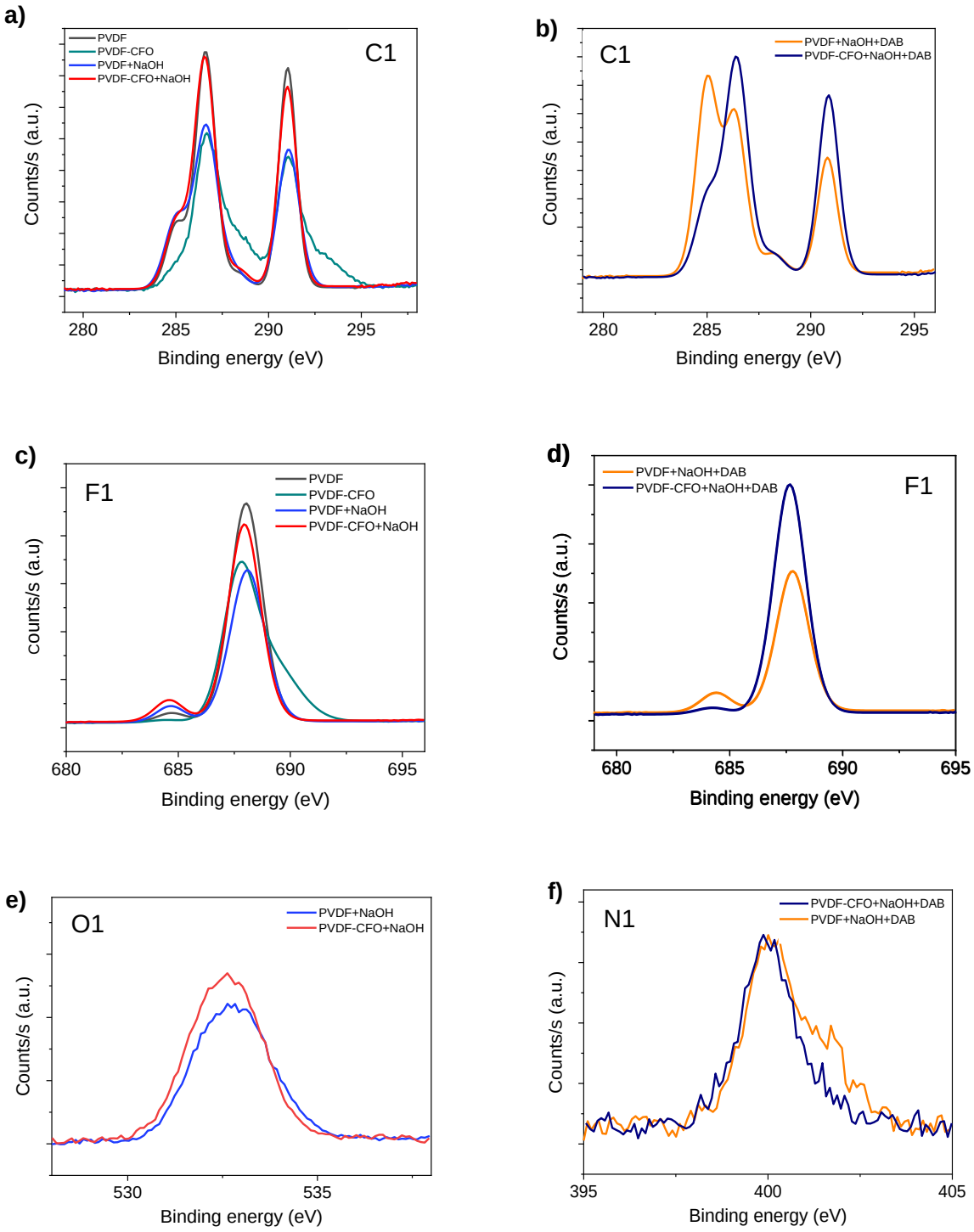

***Figure 4**. XPS spectra of untreated and chemically treated PVDF and PVDF-CFO samples C1 and F1 scan spectra for PVDF and PVDF-CFO after NaOH (a), (c), and DAB treatments (b), (d), respectively. O1 and N1 spectra for PVDF and PVDF-CFO after the NaOH treatment (e) and DAB (f).*

The quantitative elemental composition of PVDF and PVDF-CFO composites before and after the chemical treatments are summarized in Table 1, in which surface chemical modifications can be

checked. No significant changes were found in the elemental composition of the surfaces of untreated PVDF and PVDF-CFO composites, nor were there significant changes in the amount of carbon atoms, but the number of fluorine atoms dropped, accompanied by small numbers of oxygen atoms from the dehydrofluorination process, as reported in [49]. The NaOH treatment reduced the F/C ratio from 0.92 to 0.84 in PVDF and 0.97 to 0.86 in PVDF-CFO, indicating that NaOH treatment leads to the cleavage of the C-F and C-H bonds and promotes the formation of radicals that can be recombined, leading to the formation of C=C bonds. DAB chemical treatment also reduces the F/C ratio samples and increases the amount of carbon. As shown in Table 1, the F/C ratio drops from 0.92 to 0.52 and 0.97 to 0.72 for both PVDF and PVDF-CFO, respectively. No significant changes can be seen in the number of oxygen atoms. According to [49], the presence of nitrogen indicates that DAB are able to react with the $-CH_2-CH=CF-CH_2-$ chain, inducing the formation of an amino group.

***Table 1**. Surface chemical composition of PVDF and PVDF-CFO surface composites before and after chemical treatment.*

	Elemental composition (%)				
Surface	C1s	F	O	N	F/C
PVDF	51.9	48.1	-	-	0.92
PVDF-CFO	50.7	49.3	-	-	0.97
PVDF+NaOH	51.5	43.7	4.8	-	0.84
PVDF-CFO+NaOH	51.3	44.2	4.6	-	0.86
PVDF+NaOH+DAB	64.3	33.3		2.4	0.52
PVDF-CFO+NaOH+DAB	54.4	39.4	4.7	1.6	0.72

To verify the results obtained from the XPS surface analysis, the ninhydrin test, a colorimetric assay, was conducted to quantify the amino groups. These groups present on the membrane surface reacted with ninhydrin to form a purple compound. Quantification by the glycine calibration curve revealed that the concentration of amine groups was 30.1 ± 5.5 μmol/g for PVDF membranes and 27.7 ± 4.8 μmol/g for PVDF-CFO.

3.3. Layer-by-layer assembly

Five layers of each polyelectrolyte were deposited on the membrane smooth surface, starting with a layer of heparin and ending with collagen. This surface was chosen as cell culture support due to the high porosity of the bottom surface. In a previous study we found that PVDF membranes with porosities ranging from 80 to 85 % had very different outcomes regarding initial cell adhesion and proliferation, that is to say, small porosity differences can significatively influence cell behavior. Focusing on studying LbL effect and to exclude this parameter cells were seeded on the smooth surface [54].

Representative FESEM images after layer-by-layer assembly show good deposition and a homogenous coating on the surface of both membranes. Figure 5(1) shows PVDF and PVDF-CFO membranes before and after layer-by-layer assembly, with no difference in layer-by-layer coating due to the incorporation of CFO MNP in the polymer matrix, or even the presence of CFO aggregates on the membrane smooth surface.

FTIR spectra confirmed the FESEM images. Figure 5(2) shows representative FTIR spectra of a PVDF membrane with and without LbL. New peaks, highlighted with arrows, can be seen in the spectra of the last heparin (H5) and collagen layers (C5). FTIR graphs of PVDF-CFO membranes are not shown since the new peaks of both conditions were similar.

The most representative absorptions in the collagen α-helix are those of the amide A N-H stretching, with a peak appearing around 3330 cm^{-1}, the amide I C=O stretching at 1655 cm^{-1} and the amide II C-N stretching and N-H bending combination, typically appearing at 1550 cm^{-1} [55]. The absence of PVDF characteristic peaks in these regions made it easy to identify the previously mentioned collagen absorptions in the LbL coated membrane, starting with an intense amide A peak at 3330 cm^{-1}.

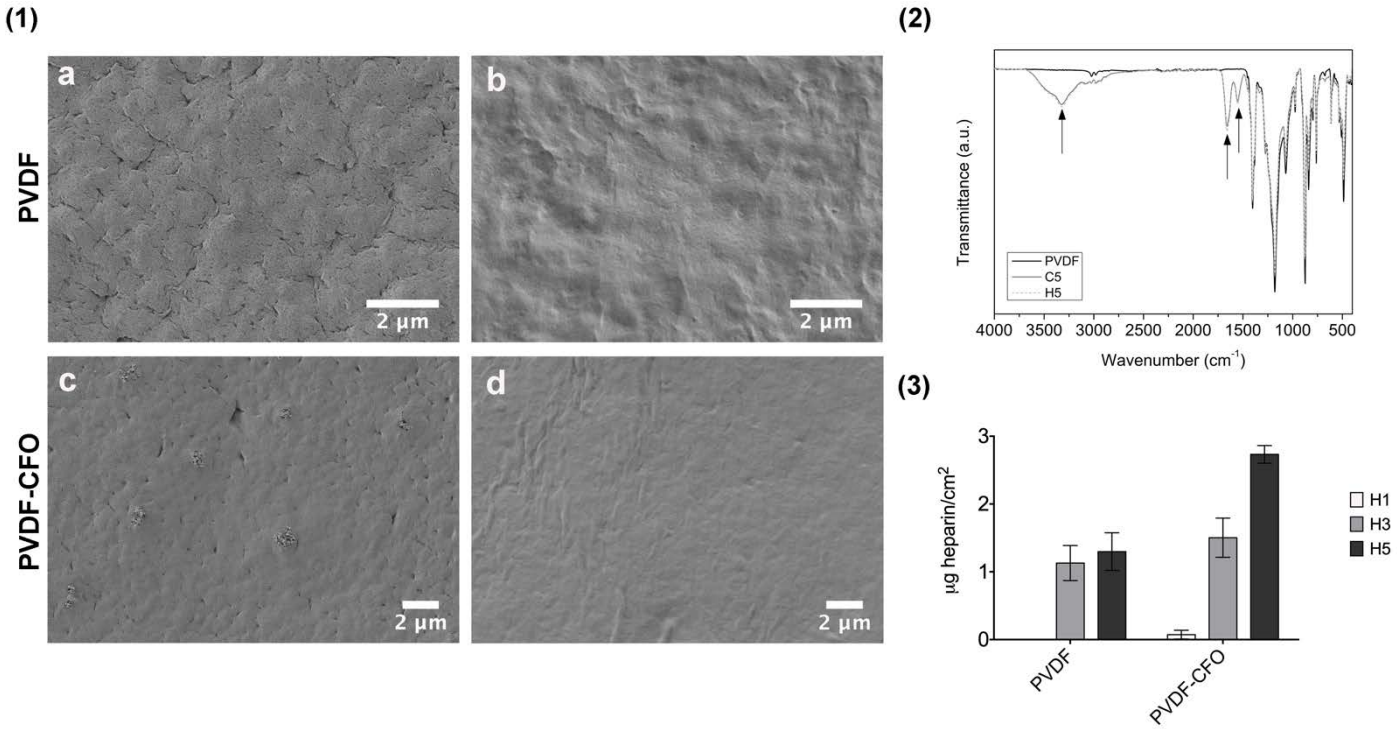

***Figure 5**. **(1)** FESEM images of layer-by-layer coating on the top surface of PVDF and PVDF-CFO membranes. **(a)** PVDF and **(c)** PVDF-CFO smooth surface without coating. **(b)** PVDF and **(d)** PVDF-CFO LbL coated surface. **(2)** FTIR spectra of PVDF membrane without LbL and PVDF membrane showing last layer of heparin (H5) and last layer of collagen (C5). Arrows highlight the characteristic peaks of the polyelectrolytes used. **(3)** Bar diagram of heparin concentration in PVDF and PVDF-CFO membranes after 1 (H1), 3 (H3) and 5 (H5) heparin layers.*

The last heparin layer spectra (dashed line) have exactly the same peaks as the last collagen layer, since proteoglycans share characteristic absorption bands with the proteins of primary and secondary amides. The C-O-S stretching band at 850 cm^{-1} cannot be distinguished due to the abundance of pronounced typical PVDF peaks in that region, especially the β-phase band at 840 cm^{-1}.

To prove heparin presence in the coated membranes, since it could not be detected by means of FTIR, heparin concentration was determined using Taylor's blue colorimetric method. As can be seen in figure 5 (3), heparin presence was only detected in the first layer of PVDF-CFO membranes, concentration of H1 in PVDF membranes was too low to be detected by this colorimetric method. After 3 layers, both types of membranes showed similar biomolecule concentrations, 1.13 ± 0.26 μg of heparin/cm^2 for PVDF membranes and 1.5 ± 0.29 μg of heparin/cm^2 in the membranes containing

CFO. The increase in heparin concentration between H1 and H3 did not follow a linear rise. This could probably be due to the presence of the subsequent layers of collagen, which provided a higher number of amine groups and positive charges than the ones obtained after amynolization, increasing the concentration of heparin deposited in the following layers. Interestingly enough, after depositing 5 layers of heparin, PVDF-CFO membranes showed a linear increase in the concentration, reaching 2.73 ± 0.13 μg of heparin/cm^2. Nonetheless, concentration of heparin was saturated after 3 layers in PVDF membranes, not showing a significant increase after the deposition of 5 layers. Differences in heparin deposition could be related with the presence of CFO, but further studies will be needed to reach a conclusion.

Deposition of collagen layers was also confirmed by atomic force microscopy. Figure 6 shows PVDF sample AFM images before and after coating with alternate layers of heparin and collagen, PVDF-C1 and PVDF-C5, for 1 and 5 bilayers respectively (from (a) to (f)). At first glance, there is not a huge difference between them when examining a large area: the height profiles at the bottom of Figure 6 are all very similar. However, there is a more subtle change which was eventually revealed by the surface roughness parameters: the more layers in the LbL process, the lower the surface roughness (R_a ranging from 28 nm for neat PVDF to 22 nm for PVDF-C5). The coating process deposits a thin layer on the PVDF surface which preferentially fills the lower parts of the topography, giving more rounded profiles with smaller differences between peaks and valleys.

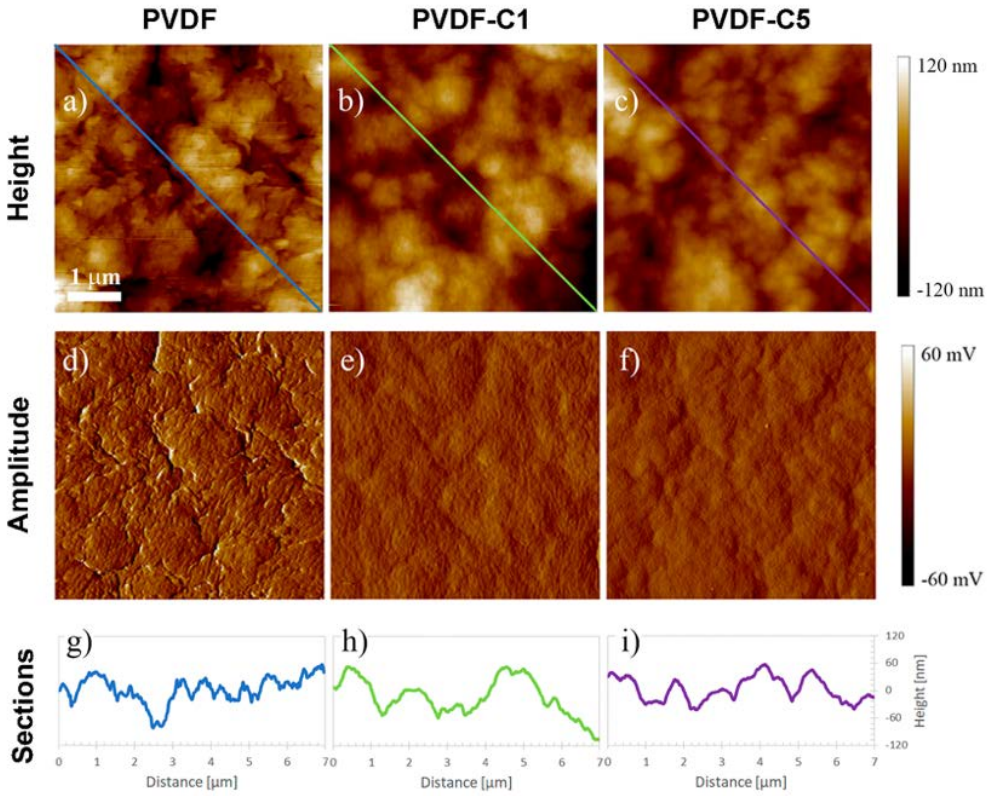

***Figure 6**. Height and amplitude AFM images of neat PVDF and PVDF coated by different numbers of alternating heparin/collagen layers (1 and 5 bilayers for C1 and C5, respectively). Height profiles of straight lines are also displayed at the bottom of the figure.*

3.4. Cell response to layer-by-layer coated membranes

Human mesenchymal stem cells were used to test initial cell response in PVDF and PVDF-CFO membranes, assuring their future use in bone tissue engineering applications. To compare the effectiveness of layer-by-layer coating, PVDF and PVDF-CFO membranes with adsorbed fibronectin were used as controls. Fibronectin is usually applied as a simple coating to favor initial cell adhesion in non-adherent biomaterials. A glass slide coated with fibronectin was also used, generally considered a standard control. A short-term culture was carried out, after 24h cell spreading was evaluated and cell number was assessed at 1, 3 and 7 days by cytoplasm-nucleus cell counting.

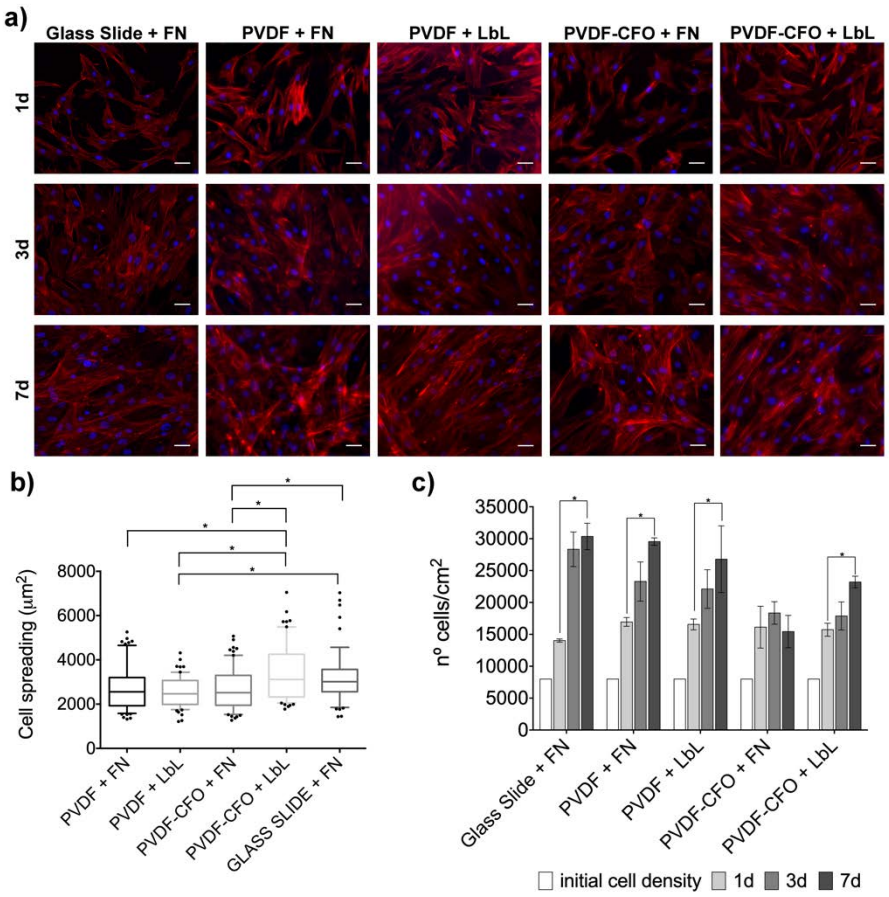

***Figure 7**. **(a)** Representative images of actin (cytoplasm-red) and Hoechst (nucleus-blue) staining after 1, 3 and 7 days of culture. High cell seeding density (8000 cells/cm^2) allows cells to reach confluence after 3 days. Scale bar is 50 µm. **(b)** Box and whiskers (10-90 percentile) of cell areas measured after 24h in each condition **(c)** Cell count based on the analysis of 4 images taken from 3 replicates per condition at 1, 3 and 7 days. * p-value < 0.05*

A high cell seeding density (8 x 10^3 cells/cm^2) was chosen. As can be seen in Figure 7(a) the cells adhered in every condition after 24h, showing well-developed cytoskeletons and fusiform morphologies typical of hMSCs. Cell spreading was assessed in every condition analyzing the images taken at the first time point studied. Figure 7 (b) shows the obtained plots. Although significant differences can be found between different conditions, they are minimal and probably associated with the heterogeneity displayed by hMSC morphologies once they adhered to the surfaces.

As indicated by the cell count, the cells duplicated within the first 24h. Cell number after 24h shows no significant differences between conditions, demonstrating the non-cytotoxic effect of CFO in the PVDF-CFO membranes at short term.

The cells continued to proliferate over time, reaching confluence after 3 days of culture, which will be the proper time to introduce external differentiation stimuli, chemical if media supplements are added or physical if differentiation is induced by electromechanical cues. In PVDF substrate not containing CFO, cells multiplied continuously up to day 7. Cell adhesion and proliferation on PVDF substrates has traditionally been ensured by a fibronectin coating on the surface, since MSC adhesion to PVDF substrates based only on the proteins adsorbed from serum is not effective. Since Ribeiro et al. [56] studied fibronectin adsorption on PVDF substrates in different crystalline phases, fibronectin has been used as a routine coating for cell culture in PVDF samples [57,58]. Coating our supports with FN attained cell numbers of the same order as glass control. Layer-by-layer coating had similar cell number after 24 h, showing that the collagen type I layer is a suitable adhesion protein for these cells.

Introducing CFO into the membrane raises the question of whether it could compromise the viability of the cells cultured on it, since cobalt ferrite oxide has been shown to be cytotoxic to human mesenchymal stem cells [59]. As can be seen in Figure 1(e), the smooth surface of PVDF-CFO membranes had some isolated CFO aggregates encapsulated in the polymer matrix. Some of them were exposed to the surface (Figure 1(f)) and could have been in contact with hMSC during the culture. Combinations of non-biodegradable polymers, as PVDF, and cobalt ferrite oxides have been previously used in cell culture approaches and its leaching has been tested [20]. The publications have shown that PVDF matrices retain CFO during cell culture, with no release of nanoparticles into the cell culture medium.

Interestingly enough, cells adhered to and were viable on PVDF-CFO supports with a fibronectin coating, since the cell number did not decrease with time. It is worth noting that no significant difference in cell spreading is shown in PVDF-CFO+FN sample with respect to glass slide + FN, and nevertheless cell number did not grow with culture time. They duplicated their numbers between seeding and day 1 but then the interaction with ferrite particles seemed to hinder further proliferation. As shown in Figure 7(c), there were no significant differences in cell numbers between days 1 and 7, although PVDF-CFO + LbL showed significant cell proliferation, indicating that the LbL coating here presented was able to cover the exposed ferrite particles (Figure 5(1-d)) hindering the direct contact

of hMSC with the CFO. LbL is effective for hMSC culture in our magnetic responsive PVDF composites produced by the NIPS technique.

These findings open the door for future cell culture approaches in bone tissue engineering using the magnetoelectric effect to induce the differentiation of human mesenchymal stem cells towards the osteogenic lineage.

4. Conclusions

NIPS has been shown to be an easy and reliable technique for producing PVDF membranes containing magnetostrictive nanoparticles for bone tissue engineering approaches. NIPS obtained electroactive membranes with a smooth surface, a thin layer with a mixture of α and β-phases, and a porous core which was completely electroactive, combining the β and γ-phases. The introduction of CFO increased the β-phase content on the surface, while reducing overall crystallinity, unlike the membranes without MNP. NIPS is an adequate technique for incorporating cobalt ferrite oxide into the polymer matrix with an MNP loss of only 10% in the manufacturing process. These membranes were aminolyzed by an alkali approach. Heparin and collagen were deposited on the membranes surface using a layer-by-layer technique, which proved to be as effective as standard fibronectin adsorption for hMSC cell culture and proliferation. LbL was also necessary for hMSC proliferation in PVDF-CFO membranes.

5. Acknowledgements

This work has been funded by the Spanish State Research Agency (AEI) and the European Regional Development Fund (ERFD) through the PID2019-106099RB-C41 / AEI / 10.13039/501100011033 and PID2019-106099RB-C43 / AEI / 10.13039/501100011033 projects and the Associate Laboratory for Green Chemistry-LAQV financed by national funds from FCT/MCTES (UIDB/50006/2020). Maria Guillot-Ferriols acknowledges the government funding of her doctoral thesis through a BES-2017-080398 FPI Grant. The CIBER-BBN initiative is funded by the VI National R&D&I Plan 2008-2011,

Iniciativa Ingenio 2010, Consolider Program. CIBER actions are financed by the *Instituto de Salud Carlos III* with assistance from the European Regional Development Fund. D.M.C is also grateful to the *FCT-Fundação para a Ciência e Tecnologia* for grant SFRH/BPD/121526/2016. Finally, the authors acknowledge funding from the Basque Government Industry and Education Department under the ELKARTEK, HAZITEK and PIBA (PIBA-2018-06) programs, respectively, also Dr. Carlos Sá (CEMUP) for assistance with the XPS analyses.

6. References

[1] J.A. McGovern, M. Griffin, D.W. Hutmacher, Animal models for bone tissue engineering and modelling disease, DMM Dis. Model. Mech. 11 (2018). https://doi.org/10.1242/dmm.033084.

[2] P. Marie, Physiology of bone tissue, Immuno-Analyse Biol. Spec. 7 (1992) 17–24. https://doi.org/10.1016/S0923-2532(05)80182-6.

[3] A. D.Woolf, B. Pfleger, Burden of major musculoskeletal conditions, Bull. World Health Organ. 81 (2003) 646–656.

[4] H.D. Kim, S. Amirthalingam, S.L. Kim, S.S. Lee, J. Rangasamy, N.S. Hwang, Biomimetic materials and fabrication approaches for bone tissue engineering, Adv. Healthc. Mater. 6 (2017) 1–18. https://doi.org/10.1002/adhm.201700612.

[5] J. Jacob, N. More, K. Kalia, G. Kapusetti, Piezoelectric smart biomaterials for bone and cartilage tissue engineering, Inflamm. Regen. 38 (2018) 1–11. https://doi.org/10.1186/s41232-018-0059-8.

[6] B.W. Kim, Clinical regenerative medicine in urology, 2017. https://doi.org/10.1007/978-981-10-2723-9.

[7] E. Fukada, I. Yasuda, On the Piezoelectric Effect of Bone, J. Phys. Soc. Japan. 12 (1957) 1158–1162.

[8] A.C. Ahn, Alan J. Grodzinsky, Relevance of collagen piezoelectricity to “Wolff’s Law”: A critical review, 31 (2010) 733–741. https://doi.org/10.1016/j.medengphy.2009.02.006.RELEVANCE.

[9] P. Martins, A.C. Lopes, S. Lanceros-Mendez, Electroactive phases of poly(vinylidene

fluoride): Determination, processing and applications, Prog. Polym. Sci. 39 (2014) 683–706. https://doi.org/10.1016/j.progpolymsci.2013.07.006.

[10] R. Gregorio, Determination of the alpha, beta, and gamma crystalline phases of poly(vinylidene fluoride) films prepared at different conditions, J. Appl. Polym. Sci. 100 (2006) 3272–3279. https://doi.org/10.1002/app.23137.

[11] V. Sencadas, R. Gregorio, S. Lanceros-Méndez, α to β phase transformation and microestructural changes of PVDF films induced by uniaxial stretch, J. Macromol. Sci. Part B Phys. 48 (2009) 514–525. https://doi.org/10.1080/00222340902837527.

[12] R. Gregorio, D.S. Borges, Effect of crystallization rate on the formation of the polymorphs of solution cast poly(vinylidene fluoride), Polymer (Guildf). 49 (2008) 4009–4016. https://doi.org/10.1016/j.polymer.2008.07.010.

[13] V. Sencadas, R. Gregorio Filho, S. Lanceros-Mendez, Processing and characterization of a novel nonporous poly(vinilidene fluoride) films in the β phase, J. Non. Cryst. Solids. 352 (2006) 2226–2229. https://doi.org/10.1016/j.jnoncrysol.2006.02.052.

[14] M.G. Buonomenna, P. Macchi, M. Davoli, E. Drioli, Poly(vinylidene fluoride) membranes by phase inversion: the role the casting and coagulation conditions play in their morphology, crystalline structure and properties, Eur. Polym. J. 43 (2007) 1557–1572. https://doi.org/10.1016/j.eurpolymj.2006.12.033.

[15] C. Ribeiro, C.M. Costa, D.M. Correia, J. Nunes-Pereira, J. Oliveira, P. Martins, R. Gonçalves, V.F. Cardoso, S. Lanceros-Méndez, Electroactive poly(vinylidene fluoride)-based structures for advanced applications, Nat. Protoc. 13 (2018) 681–704. https://doi.org/10.1038/nprot.2017.157.

[16] F. Liu, N.A. Hashim, Y. Liu, M.R.M. Abed, K. Li, Progress in the production and modification of PVDF membranes, J. Memb. Sci. 375 (2011) 1–27. https://doi.org/10.1016/j.memsci.2011.03.014.

[17] N. Abzan, M. Kharaziha, S. Labbaf, Development of three-dimensional piezoelectric polyvinylidene fluoride-graphene oxide scaffold by non-solvent induced phase separation method for nerve tissue engineering, Mater. Des. 167 (2019) 107636.

https://doi.org/10.1016/j.matdes.2019.107636.

[18] T.H. Young, H.H. Chang, D.J. Lin, L.P. Cheng, Surface modification of microporous PVDF membranes for neuron culture, J. Memb. Sci. 350 (2010) 32–41. https://doi.org/10.1016/j.memsci.2009.12.009.

[19] R. Gonçalves, P. Martins, D.M. Correia, V. Sencadas, J.L. Vilas, L.M. León, G. Botelho, S. Lanceros-Méndez, Development of magnetoelectric CoFe2O4/poly(vinylidene fluoride) microspheres, RSC Adv. 5 (2015) 35852–35857. https://doi.org/10.1039/C5RA04409J.

[20] M.M. Fernandes, D.M. Correia, C. Ribeiro, N. Castro, V. Correia, S. Lanceros-Mendez, Bioinspired Three-Dimensional Magnetoactive Scaffolds for Bone Tissue Engineering, ACS Appl. Mater. Interfaces. 11 (2019) 45265–45275. https://doi.org/10.1021/acsami.9b14001.

[21] B. Hermenegildo, C. Ribeiro, L. Pérez-Álvarez, J.L. Vilas, D.A. Learmonth, R.A. Sousa, P. Martins, S. Lanceros-Méndez, Hydrogel-based magnetoelectric microenvironments for tissue stimulation, Colloids Surfaces B Biointerfaces. 181 (2019) 1041–1047. https://doi.org/10.1016/j.colsurfb.2019.06.023.

[22] R. Gonçalves, P. Martins, X. Moya, M. Ghidini, V. Sencadas, G. Botelho, N.D. Mathur, S. Lanceros-Mendez, Magnetoelectric $CoFe_2O_4$ /polyvinylidene fluoride electrospun nanofibres, Nanoscale. 7 (2015) 8058–8061. https://doi.org/10.1039/C5NR00453E.

[23] J. Silva, R.R. Costa, J.F. Mano, Biomimetic Extracellular Environment Based on Natural Origin Polyelectrolyte Multilayers, Small. 12 (2016) 4301–4439.

[24] R.R. Costa, J.F. Mano, Polyelectrolyte multilayered assemblies in biomedical technologies, Chem. Soc. Rev. 43 (2014) 3453–3479. https://doi.org/10.1039/c3cs60393h.

[25] D.A. Castilla-Casadiego, L. Pinzon-Herrera, M. Perez-Perez, B.A. Quiñones-Colón, D. Suleiman, J. Almodovar, Simultaneous characterization of physical, chemical, and thermal properties of polymeric multilayers using infrared spectroscopic ellipsometry, Colloids Surfaces A Physicochem. Eng. Asp. 553 (2018) 155–168. https://doi.org/10.1016/j.colsurfa.2018.05.052.

[26] R.F. Mhanna, J. VörÖs, M. Zenobi-Wong, Layer-by-layer films made from extracellular matrix macromolecules on silicone substrates, Biomacromolecules. 12 (2011) 609–616.

https://doi.org/10.1021/bm1012772.

[27] P.C. Billings, M. Pacifici, Interactions of signaling proteins, growth factors and other proteins with heparan sulfate: Mechanisms and mysteries, Connect. Tissue Res. 56 (2015) 272–280. https://doi.org/10.3109/03008207.2015.1045066.

[28] K. Zhang, J. ying Chen, W. Qin, J. an Li, F. xia Guan, N. Huang, Constructing bio-layer of heparin and type IV collagen on titanium surface for improving its endothelialization and blood compatibility, J. Mater. Sci. Mater. Med. 27 (2016). https://doi.org/10.1007/s10856-016-5693-6.

[29] W.J. Cherng, Y.H. Pan, T.C. Wu, C.C. Chou, C.H. Yeh, J.J. Ho, Hemocompatibility and adhesion of heparin/dopamine and heparin/collagen self-assembly multilayers coated on a titanium substrate, Appl. Surf. Sci. 463 (2019) 732–740. https://doi.org/10.1016/j.apsusc.2018.08.217.

[30] J. Chen, N. Huang, Q. Li, C.H. Chu, J. Li, M.F. Maitz, The effect of electrostatic heparin/collagen layer-by-layer coating degradation on the biocompatibility, Appl. Surf. Sci. 362 (2016) 281–289. https://doi.org/10.1016/j.apsusc.2015.11.227.

[31] K. Zhang, D. Huang, Z. Yan, C. Wang, Heparin/collagen encapsulating nerve growth factor multilayers coated aligned PLLA nanofibrous scaffolds for nerve tissue engineering, J. Biomed. Mater. Res. - Part A. 105 (2017) 1900–1910. https://doi.org/10.1002/jbm.a.36053.

[32] A.M. Ferreira, P. Gentile, S. Toumpaniari, G. Ciardelli, M.A. Birch, Impact of Collagen/Heparin Multilayers for Regulating Bone Cellular Functions, ACS Appl. Mater. Interfaces. 8 (2016) 29923–29932. https://doi.org/10.1021/acsami.6b09241.

[33] K. Jin, B. Li, L. Lou, Y. Xu, X. Ye, K. Yao, J. Ye, C. Gao, In vivo vascularization of MSC-loaded porous hydroxyapatite constructs coated with VEGF-functionalized collagen/heparin multilayers, Sci. Rep. 6 (2016) 1–13. https://doi.org/10.1038/srep19871.

[34] D.A. Castilla-Casadiego, J.R. García, A.J. García, J. Almodovar, Heparin/Collagen Coatings Improve Human Mesenchymal Stromal Cell Response to Interferon Gamma, ACS Biomater. Sci. Eng. 5 (2019) 2793–2803. https://doi.org/10.1021/acsbiomaterials.9b00008.

[35] P. Martins, R. Gonçalves, S. Lanceros-Mendez, A. Lasheras, J. Gutiérrez, J.M. Barandiarán,

Effect of filler dispersion and dispersion method on the piezoelectric and magnetoelectric response of CoFe 2 O 4 /P(VDF-TrFE) nanocomposites, Appl. Surf. Sci. 313 (2014) 215–219. https://doi.org/10.1016/j.apsusc.2014.05.187.

[36] T.C. Gamboa-Martínez, V. Luque-Guillén, C. González-García, J.L. Gõmez Ribelles, G. Gallego-Ferrer, Crosslinked fibrin gels for tissue engineering: Two approaches to improve their properties, J. Biomed. Mater. Res. - Part A. 103 (2015) 614–621. https://doi.org/10.1002/jbm.a.35210.

[37] R. Gregorio, M. Cestari, Effect of crystallization temperature on the crystalline phase content and morphology of poly(vinylidene fluoride), J. Polym. Sci. Part B Polym. Phys. 32 (1994) 859–870. https://doi.org/10.1002/polb.1994.090320509.

[38] P. Martins, C.M. Costa, S. Lanceros-Mendez, Nucleation of electroactive β-phase poly(vinilidene fluoride) with CoFe2O4 and NiFe2O4 nanofillers: A new method for the preparation of multiferroic nanocomposites, Appl. Phys. A Mater. Sci. Process. 103 (2011) 233–237. https://doi.org/10.1007/s00339-010-6003-7.

[39] L. Qi, E.K. Knapton, X. Zhang, T. Zhang, C. Gu, Y. Zhao, Pre-culture Sudan Black B treatment suppresses autofluorescence signals emitted from polymer tissue scaffolds, Sci. Rep. 7 (2017) 8361. https://doi.org/10.1038/s41598-017-08723-2.

[40] T.H. Young, L.P. Cheng, D.J. Lin, L. Fane, W.Y. Chuang, Mechanisms of PVDF membrane formation by immersion-precipitation in soft (1-octanol) and harsh (water) nonsolvents, Polymer (Guildf). 40 (1999) 5315–5323. https://doi.org/10.1016/S0032-3861(98)00747-2.

[41] L.P. Cheng, Effect of temperature on the formation of microporous PVDF membranes by precipitation from 1-Octanol/DMF/PVDF and water/ DMF/PVDF systems, Macromolecules. 32 (1999) 6668–6674. https://doi.org/10.1021/ma990418l.

[42] S. Supriya, L. Kumar, M. Kar, Optimization of dielectric properties of PVDF–CFO nanocomposites, Polym. Compos. 40 (2019) 1239–1250. https://doi.org/10.1002/pc.24840.

[43] D.J. Lin, K. Beltsios, T.H. Young, Y.S. Jeng, L.P. Cheng, Strong effect of precursor preparation on the morphology of semicrystalline phase inversion poly(vinylidene fluoride) membranes, J. Memb. Sci. 274 (2006) 64–72. https://doi.org/10.1016/j.memsci.2005.07.043.

[44] X. Cai, T. Lei, D. Sun, L. Lin, A critical analysis of the α, β and γ phases in poly(vinylidene fluoride) using FTIR, RSC Adv. 7 (2017) 15382–15389. https://doi.org/10.1039/c7ra01267e.

[45] T. Boccaccio, A. Bottino, G. Capannelli, P. Piaggio, Characterization of PVDF membranes by vibrational spectroscopy, J. Memb. Sci. 210 (2002) 315–329. https://doi.org/10.1016/S0376-7388(02)00407-6.

[46] J. Liu, X. Lu, C. Wu, Effect of preparation methods on crystallization behavior and tensile strength of poly(vinylidene fluoride) membranes, Membranes (Basel). 3 (2013) 389–405. https://doi.org/10.3390/membranes3040389.

[47] M. Zhang, A.Q. Zhang, B.K. Zhu, C.H. Du, Y.Y. Xu, Polymorphism in porous poly(vinylidene fluoride) membranes formed via immersion precipitation process, J. Memb. Sci. 319 (2008) 169–175. https://doi.org/10.1016/j.memsci.2008.03.029.

[48] L. Xiao, D.M. Davenport, L. Ormsbee, D. Bhattacharyya, Polymerization and functionalization of membrane pores for water related applications, Ind. Eng. Chem. Res. 54 (2015) 4174–4182. https://doi.org/10.1021/ie504149t.

[49] C. Algieri, L. Donato, L. Giorno, Tyrosinase immobilized on a hydrophobic membrane, Biotechnol. Appl. Biochem. 64 (2017) 92–99. https://doi.org/10.1002/bab.1462.

[50] M.D. Duca, C.L. Plosceanu, T. Pop, Effect of X-rays on Poly(vinylidene fluoride) in X-ray Photoelectron Spectroscopy, J. Appl. Polym. Sci. 67 (1998) 2125–2129.

[51] D.M. Correia, C. Ribeiro, V. Sencadas, G. Botelho, S.A.C. Carabineiro, J.L.G. Ribelles, S. Lanceros-Méndez, Influence of oxygen plasma treatment parameters on poly(vinylidene fluoride) electrospun fiber mats wettability, Prog. Org. Coatings. 85 (2015) 151–158. https://doi.org/10.1016/j.porgcoat.2015.03.019.

[52] I.-S. Lim, S.-H. Yoo, I.-N. Park, Y.-S. Lee, Influence of Oxyfluorination on Properties of Polyacrylonitrile (PAN)- Based Carbon Fibers, Carbon Lett. 5 (2004) 12–17.

[53] M. Kehrer, J. Duchoslav, A. Hinterreiter, M. Cobet, A. Mehic, T. Stehrer, D. Stifter, XPS investigation on the reactivity of surface imine groups with TFAA, Plasma Process. Polym. 16 (2019) 1–8. https://doi.org/10.1002/ppap.201800160.

[54] R.M. Morales-Román, M. Guillot-Ferriols, L. Roig-Pérez, S. Lanceros-Mendez, G. Gallego-

Ferrer, J.L. Gómez Ribelles, Freeze-extraction microporous electroactive supports for cell culture, Eur. Polym. J. 119 (2019) 531–540. https://doi.org/10.1016/j.eurpolymj.2019.07.011.

[55] N.P. Camacho, P. West, P.A. Torzilli, R. Mendelsohn, FTIR microscopic imaging of collagen and proteoglycan in bovine cartilage, Biopolym. - Biospectroscopy Sect. 62 (2001) 1–8. https://doi.org/10.1002/1097-0282(2001)62:1<1::AID-BIP10>3.0.CO;2-O.

[56] C. Ribeiro, J.A. Panadero, V. Sencadas, S. Lanceros-Méndez, M.N. Tamaño, D. Moratal, M. Salmerón-Sánchez, J.L. Gómez Ribelles, Fibronectin adsorption and cell response on electroactive poly(vinylidene fluoride) films, Biomed. Mater. 7 (2012). https://doi.org/10.1088/1748-6041/7/3/035004.

[57] C. Ribeiro, J. Pärssinen, V. Sencadas, V. Correia, S. Miettinen, V.P. Hytönen, S. Lanceros-Méndez, Dynamic piezoelectric stimulation enhances osteogenic differentiation of human adipose stem cells, J. Biomed. Mater. Res. - Part A. 103 (2015) 2172–2175. https://doi.org/10.1002/jbm.a.35368.

[58] R. Sobreiro-Almeida, M. Tamaño-Machiavello, E. Carvalho, L. Cordón, S. Doria, L. Senent, D. Correia, C. Ribeiro, S. Lanceros-Méndez, R. Sabater i Serra, J. Gomez Ribelles, A. Sempere, Human Mesenchymal Stem Cells Growth and Osteogenic Differentiation on Piezoelectric Poly(vinylidene fluoride) Microsphere Substrates, Int. J. Mol. Sci. 18 (2017) 2391. https://doi.org/10.3390/ijms18112391.

[59] S. Moise, E. Céspedes, D. Soukup, J.M. Byrne, A.J. El Haj, N.D. Telling, The cellular magnetic response and biocompatibility of biogenic zinc- and cobalt-doped magnetite nanoparticles, Sci. Rep. 7 (2017) 1–11. https://doi.org/10.1038/srep39922.